Droplet-ambient sub-grid interaction modeling in large eddy simulation of diesel sprays

Nidheesh Bharadwaj* and Christopher Rutland
Engine Research Center
University of Wisconsin-Madison
Madison, WI 53706 USA

Abstract

This work presents a large eddy simulation (LES) study of diesel sprays and particle laden flows. A one-equation dynamic structure LES model is used which solves an additional transport equation for sub-grid kinetic energy (k). The atomized liquid droplets are generally smaller than the computational cell, and therefore the sub-grid scale interaction of droplets with the ambient gas phase needs to be modeled in the LES of diesel sprays. This two-phase interaction is accounted through the spray source term in the k_{sgs} - transport equation. The spray source term is a dot product of the droplet drag and the gas phase sub-grid gas velocity. An approximate deconvolution technique is used to obtain the sub-grid velocities from the resolved flow field. The results of the LES predicted mean and turbulence velocities for a particle laden jet are shown to compare very well with the previous experiments. A discussion on the sub-grid, resolved, turbulence and mean kinetic energies is presented. The non-evaporating diesel spray LES results are compared with previously published X-ray radiography experiments conducted at Argonne National Laboratory. The comparisons are made for quantities such as transverse integrated mass (TIM), mass averaged axial velocity profile and spray momentum.

* Corresponding author: nbharadwaj@wisc.edu

Introduction

An engine flow consists of a vast range of turbulence scales, ranging from droplet size (a few micrometers) to cylinder diameter (several centimeters). Direct Numerical Simulation (DNS) of such complex flows requires an enormous amount of computational expense and is impractical based on the current computational limitations. In Large Eddy Simulation (LES), depending upon the spatial filter size, large scale turbulence is resolved while the unresolved small scale turbulence is modeled. LES has the ability to capture the local unsteadiness of the flow. Such unsteady details of a flow are lost in another turbulence modeling technique, called, Reynolds Averaged Navier Stokes (RANS) simulations which solve ensemble averaged governing equations. Due to its ability to provide much more detailed flow information than RANS, on grids which are still much coarser than those required for DNS, LES has received a lot of attention in both fundamental and practical research communities. In the context of diesel engines, the knowledge of spray-gas turbulent interaction is crucial in gaining a detailed understanding of the combustion characteristics, and hence, this study is focused on LES model development and validation of the two-phase turbulence interaction between high pressure liquid diesel sprays and the gas phase turbulent field.

Since the droplets interact with very small gas phase length scales, the LES of sprays presents new conceptual challenges. There have been several LES studies on particle laden flows that consistently showed the ability of LES to provide reasonably accurate predictions in varied flow configurations. For example, using a one way coupling (from gas to particle), Armenio *et al* [1] compared particle dispersion from fully resolved DNS velocity field with that from filtered DNS velocities and found that the results became poorer with increasing filter size. A priori and a posteriori studies of particle laden mixing layers by Okong'o and Bellan [2] and Leboissetier *et al* [3] showed that similarity and dynamic LES models predicted better turbulent statistics than constant and dynamic coefficient based Smagorinsky models. In their LES *a priori* study Okong'o and Bellan [2] pointed out that for particle laden flows, the droplets provided a significant contribution to the gas phase kinetic energy. Calibrated sub-grid stress coefficients based on this *a priori* study were later successfully used in an *a posteriori* study by Leboissetier *et al* [4].

Stolz and Adams [5] and Stolz *et al* [6] developed an approximate deconvolution technique (ADM) for the reconstruction of unfiltered velocity field based on LES filtered velocities. Shotorban and Mashayek [7] and Shotorban *et al* [8] later showed consistent improvement in their results for particle laden homogeneous shear flows by using this deconvolution technique for correcting sub-grid velocity field for drop drag calculations. In a recent work, Bharadwaj *et al* [9] derived a k_{sgs} transport equation using a LES specific two phase filtering procedure (see Sirignano [10]). A model for the unclosed spray source term was then proposed. The model was applied in an LES study of evaporative diesel sprays and was found to have a significant improvement in spray penetration results.

This study uses a dynamic structure non-viscosity LES model (Pomraning and Rutland [11]) in which sub-grid shear stress calculation is based on sub-grid kinetic energy (k_{sgs}) obtained from a transport equation. The non-viscosity LES approach is different than a viscosity LES approach in which sub-grid stress tensor is related to filtered strain rate using an eddy viscosity. Sub-grid kinetic energy is also used for droplet turbulent dispersion. In the current work, the LES spray source model from Bharadwaj *et al* [9] is applied to a particle laden gas jet and high speed non-evaporative diesel sprays. The primary focus of the current work is to analyze sub-grid scale turbulence effects caused by the particle phase, and assess two-phase LES results through comparisons with previous experiments of Gillandt et al [12] for particles laden gas jet and Kastengren et al [13, 14] for non-evaporative diesel sprays.

The rest of this paper is organized as follows. First, the basic gas-phase LES models in the LES filtered equations are provided. Then, the modeling approach for the spray source term in the sub-grid kinetic energy transport equation is discussed. The Lagrangian point parcel approach and the phenomenological spray models are provided next. Then the simulation results are discussed for a particle laden gas jet and high speed diesel spray cases. Finally, a conclusion is given at the end.

LES Gas Phase Models

LES filtered mass, momentum, internal energy, species transport, and sub-grid kinetic energy equations [9] are solved in the KIVA-3v release 2 code [15, 16]. The closure of the sub-grid shear stress term is based on the dynamic structure one-equation non-viscosity model given by Pomraning and Rutland [11]. According to this model, sub-grid shear stress is calculated as $\Gamma_{ij} = c_{ij} k_{sgs}$, where k_{sgs} is the sub-grid kinetic energy discussed below. Using Germano identity [17], the tensor coefficient c_{ij} is calculated as $c_{ij} = L_{ij} / L_{kk}$ where L_{ij} is the Leonard stress tensor that relates the filter level and test filter level velocities as:

$$L_{ij} = \widehat{\langle u_i \rangle \langle u_j \rangle} - \widehat{\langle u_i \rangle} \widehat{\langle u_j \rangle},$$

where the operator $\widehat{\ }$ implies a test level filter. The unclosed sub-grid scale dissipation rate term in the resolved internal energy is equal to the dissipation rate term of the sub-grid kinetic energy equation. Using a turbulent viscosity approach (Menon [18]), the unclosed sub-grid heat flux in the resolved scalar transport equation is modeled as

$$h_j^{sgs} = -\left(\mu_T C_p / \mathrm{Pr}_T\right) \partial T / \partial x_j,$$

and the sub-grid species flux is modeled as

$$\Phi_{j,k}^{sgs} = -(\mu_T / Sc_T) \partial \langle Y_k \rangle / \partial x_j.$$

Turbulent Prandtl and Schmidt numbers are prescribed as $\mathrm{Pr}_T = 1$ and $Sc_T = 1$. The relation for turbulent viscosity is given below. The spray contributions to gas phase equations appear as the source terms of mass, momentum, and energy. Please see references [2, 4, 9] for a detailed discussion on the basic two-phase coupling in the gas phase conservation equations.

LES Spray Source Modeling

The two-phase turbulence interaction is accounted through the spray source term in the transport equation of the sub-grid kinetic energy, and a response of turbulence towards the sub-grid scale droplet motion is accounted through turbulence dispersion. The following transport equation of k_{sgs} is solved in the KIVA code [15]

$$\frac{\partial \bar{\rho} k_{sgs}}{\partial t} + \frac{\partial \bar{\rho} \langle u_j \rangle k_{sgs}}{\partial x_j} = -\frac{\partial}{\partial x_j}\left(\mu_T \frac{\partial k_{sgs}}{\partial x_j}\right) + P - \varepsilon_{sgs} + \dot{W}_{s,sgs}, \quad (1)$$

The dissipation rate and turbulent viscosity are modeled as $\varepsilon_{sgs} = C_1 \bar{\rho} k_{sgs}^{3/2} / \Delta$ and $\mu_T = C_2 \bar{\rho} \Delta k_{sgs}^{1/2}$. In these relations, Δ is the filter (or grid) size, $C_1 = 0.05$ and $C_2 = 0.3$. The production term, $P = -\Gamma_{ij} S_{ij}$ where Γ_{ij} is the sub-grid shear stress and S_{ij} is the filtered strain rate.

The spray source term, $\dot{W}_s$, is modeled as a dot product of the filtered drag and the gas phase sub-grid velocity,

$$\dot{W}_s = -F_i u_i^{sgs}. \quad (2)$$

The sub-grid velocity, u_i^{sgs}, is obtained after applying an approximate de-convolution on the filtered gas velocity. Assuming that the inverse of the filtering function, G^{-1}, exists; first obtain the unfiltered gas velocity as [5, 6]

$$u_i = G^{-1} * \langle u_i \rangle = \sum_{\alpha=0}^{N} (I - G)^{\alpha} \langle u_i \rangle = \langle u_i \rangle + \left(\langle u_i \rangle - \langle\langle u_i \rangle\rangle\right) + \left(\langle u_i \rangle - 2\langle\langle u_i \rangle\rangle + \langle\langle\langle u_i \rangle\rangle\rangle\right) + \ldots, \quad (3)$$

and then, obtain the sub-grid velocity as

$$u_i^{sgs} \equiv u_i - \langle u_i \rangle. \quad (4)$$

The first three terms in the above series expansion have been found sufficient to give good predictions in pervious studies [5-8]. Hence, the sub-grid velocity is finally modeled as

$$u_i^{sgs} = 2\langle u_i \rangle - 3\langle\langle u_i \rangle\rangle + \langle\langle\langle u_i \rangle\rangle\rangle. \quad (5)$$

The extra brackets in this equation imply additional filtering applied through a test filter formed by an extra cell layer around the cell being filtered. The filtered droplet drag is obtained as

$$F_i = \frac{\sum_d F_{i,d}}{V_{cell}}, \quad (6)$$

where $F_{i.d}$ is the drag on each droplet lying within the cell of volume V_{cell}, and the summation is over all droplets within the cell. The aerodynamic model for droplet drag [15] is

$$F_{i,d} = \frac{3}{8} \frac{\bar{\rho}}{\rho_l} \frac{m_d V_{rel}}{r_d} \left(\langle u_i \rangle + u'_{p,i} - v_{d,i}\right) C_D, \quad (7)$$

where ρ_l, r_d, m_d, $v_{d,i}$ and C_D are the liquid droplet density, radius, mass, velocity and drag coefficient, respectively, and $u'_{p,i}$ is the droplet turbulent dispersion velocity based on a Gaussian (or locally isotropic) relation with the standard deviation proportional to $\sqrt{k_{sgs}}$ [9].

Lagrangian Formulation and Spray Models

The diesel spray is assumed to be composed of discrete liquid droplets. For numerical efficiency, several droplets with the same size and location are treated together in the form of a computational parcel. The droplets are tracked using Lagrangian equations of motion coupled with mass and energy balance [15]. A point parcel approach is utilized in which the droplets are invisible to the surrounding gas phase. This approach is based on the assumption that the size of a droplet is much smaller then the size of the surrounding gas phase eddy. The primary and secondary break-up processes are modeled using a hybrid Kelvin Helmholtz (KH) – Rayleigh Taylor (RT) model [19]. The droplet

collision is based on O'Rourke's model [20]. The spray is injected using the blob injection model [21] in which the liquid core is represented by the droplet parcels.

Simulation Results and Discussion

The results and discussion are presented for particle laden flows and diesel sprays. The focus is on the mean and fluctuation characteristics, the estimates on the resolved and sub-grid scales, and comparison of the results with the available experiments. These issues are covered in the following sub-sections by presenting results for (i) a particle laden stationary turbulent gas jet case and (ii) non-evaporative high speed diesel spray cases.

Particle Laden Gas Jet

This section presents LES results from a single phase and a two phase (particle laden) gas jet. The simulation conditions are taken from the Phase-Doppler-Anemometry (PDA) measurements of Gillandt *et al* [12] (see Table 1). The two phase jet in the experiment was obtained by seeding the single phase jet with glass beads (mean particle size 110 μm . The velocity measurements in both single and two phase jets were based on tracer silica particle (size 1). The particle size statistics in the present simulations is mimicked using a Rosin-Rammler distribution around 110 μm . The droplet injection location is uniformly distributed within the inlet area at a mass loading ratio of one. The mean velocity at the pipe exit (inlet in the simulations) for the gas jet is $U_{jet} = 7.7\text{m/s}$, and for the particles is $U_{p,jet} = 0.85U_{jet}$.

Table 1 Measurement conditions for particle laden gas jet

Reynolds number	5700
Tube diameter	12mm
Particles	Glass bead
Mean particle diameter	110 μm
Mass loading	1

The simulations are conducted in a cylindrical domain of diameter 20 cm and length 25 cm. The peripheral wall and the wall around the inlet are specified with a free slip boundary condition and the exit boundary an outflow condition. The CFD mesh is shown in Figure 1. The mesh contains a total of 0.5 million cells where 200 cells are in the axial direction. The mesh structure in the jet inlet plane ($D < D_{jet}$) has a Cartesian form with 8^2 cells, and in the outside region has a polar form with an additional 21 azimuthal cell layers. There are overall 2500 cells in the cross-flow plane. The grid density is highest in the core jet region and decreases towards the wall.

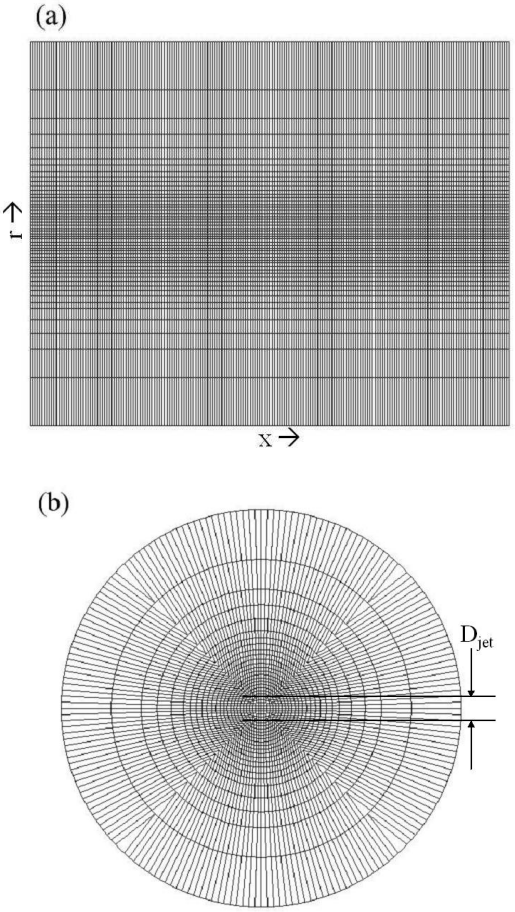

Figure 1 Front (a) and top (b) views of the mesh used for gas jet simulations. The dimensions of the cylinder are 20cm (diameter) x 25cm (length).

Figure 2 shows a qualitative picture of the particle laden jet simulation. In this figure an iso-surface of the second invariant of vorticity at an arbitrarily chosen value of $3\times10^3\text{cm}^2/\text{s}^2$ is overlaid by injected species mass fraction to elaborate the flow structures. This figure highlights the capability of LES to predict both the initial intermittency and the large scale coherent turbulent structures. The particles are shown as small discrete color contours. The figure also shows that heavy particles tend to maintain their inertia throughout their travel where as the lighter particles lose their initial inertia and disperse radially outward. The size (and color) of discrete spheres is proportional to the size of the physical particles.

The simulations are run for three flow pass-through times (~0.3s) and the mean statistics are evaluated during the final flow through time. Since the flow is homogeneous in the azimuthal direction, the mean data

is shown only in the half radial plane where each value is averaged in time and in the azimuthal direction (represented by an overbar).

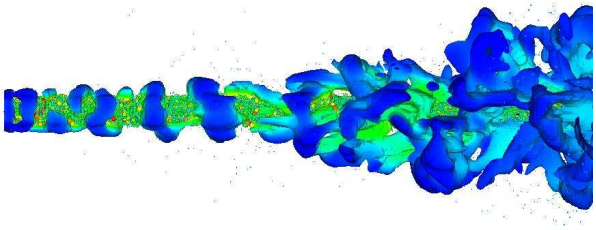

Figure 2 Qualitative picture of the particle laden gas jet simulation showing iso-contours of the second invariant of vorticity at a value of 3.0×10^3 cm^2/s^2 overlaid by mass fraction of injected species (air).

Figure 3 compares the LES predictions with experiments for the radial profiles of the normalized axial mean and fluctuation velocity at $x - x_0$ equal to 3, 6 and 9cm. This figure confirms the ability of LES to accurately predict both measured velocity mean and fluctuations over a range of axial and radial locations. Since the single phase and the two phase gas jets start with the same initial velocities, the gas phase mean velocities for the two cases are similar initially and differ in the downstream direction due to particle inertia effects. The fluctuation profiles show that the high inertia particles in the central region slightly decrease the fluctuation in comparison with the single phase jet. This is because of the 'crossing trajectory' effect of the particles in which particles trajectories cut through the small gas phase turbulent eddies, thereby decreasing the fluctuating velocity correlations and hence the turbulence levels (Gillandt *et al* [12]).

Figure 4 shows the probability distribution functions (PDF) plots of the spray source term in two separate regions: (a) $x - x_o < 6\text{cm}$ and (b) $6 < x - x_o < 12\text{cm}$. This figure shows that the magnitudes of $\dot{W}_{s,sgs}$ in the upstream region are higher and distributed more on the negative side, whereas those in the downstream region of are smaller and distributed slightly more on the positive side. This shifting in the sign of $\dot{W}_{s,sgs}$ is a consequence of the dot product between the drag force and the sub-grid velocity. The solid particles, due to their higher inertia than the gas phase, lose momentum at a much slower rate. Therefore, recalling that the particles are injected with a smaller (85%) velocity than the gas phase, the particle velocities remain smaller than the gas velocities only up to a certain axial location and become higher afterwards. This cross over in the relative velocity sign takes place at approximately $x - x_o \approx 6\text{cm}$ (not shown here), and is mainly responsible for the $\dot{W}_{s,sgs}$ distribution shifting from negative to positive downstream.

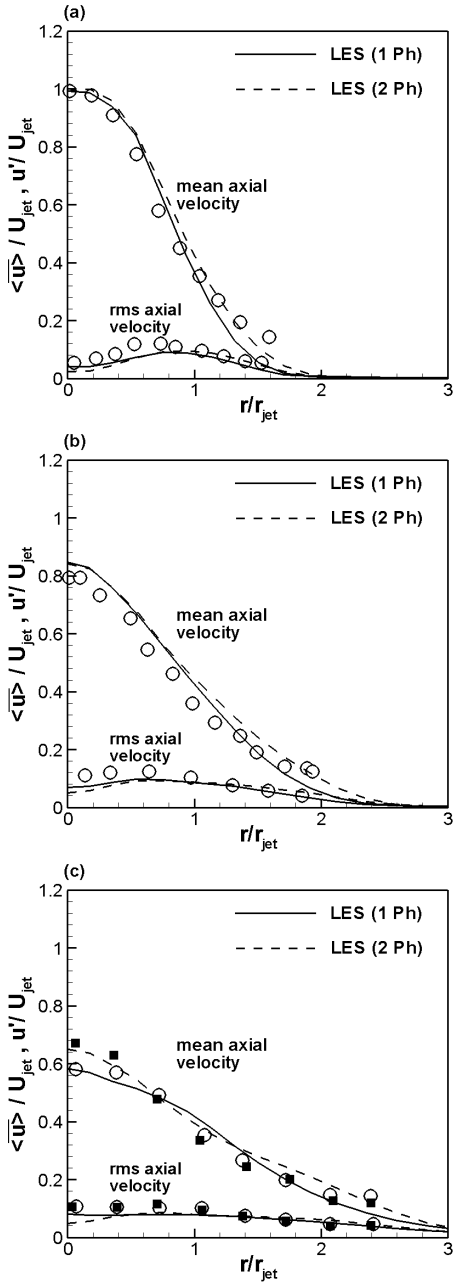

Figure 3 Radial profiles of mean and fluctuation axial velocity at $x - x_o = 3\text{cm}$ (a), 6cm (b), 9cm (c) and 15cm (d). Experimental results are shown by symbols: circles for single phase (1Ph) and squares for two phase (2 Ph). For (a) and (b) experimental two phase results were not discernible from single phase results and hence not shown here. Experiments are from Gillandt *et al* [12]

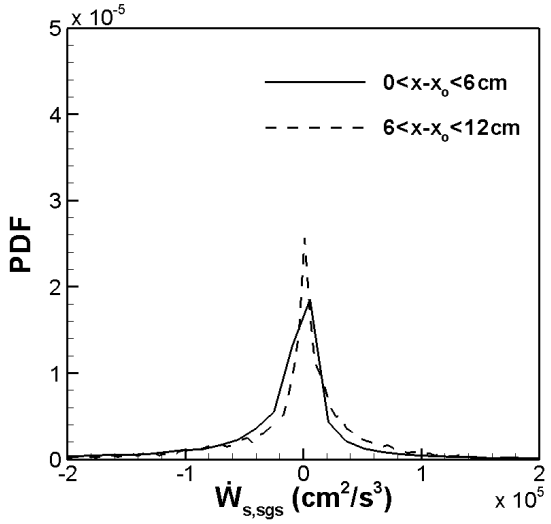

Figure 4 PDF of sub-grid spray source term in two separate downstream regions for the particle laden gas jet.

Therefore, recalling that the particles are injected with a smaller (85%) velocity than the gas phase, the particle velocities remain smaller than the gas velocities only up to a certain axial location and become higher afterwards. This cross over in the relative velocity sign takes place at approximately $x - x_o \approx 6\text{cm}$ (not shown here), and is mainly responsible for the $\dot{W}_{s,sgs}$ distribution shifting from negative to positive downstream.

Relative order of magnitudes of resolved (k_{res}), mean (k_{mean}), sub-grid (k_{sgs}) and turbulence (TKE) kinetic energies can provide additional insight. The axial variations of these quantities are shown in Figure 5 both for single and two phase flows at a specific instant. Here, the TKE is approximated by the variance of the LES resolved kinetic energy fluctuation about its mean. The resolved kinetic energy is fluctuating around the mean since the mean velocities are calculated from the resolved velocities. It is interesting to notice that the downstream TKE in the two phase flow is less than the single phase flow, whereas the downstream k_{sgs} in the two phase flow is higher than the single phase flow. This is consistent with the 'crossing trajectory' effect and the spray source term ($\dot{W}_{s,sgs}$) effects discussed previously. Figure 5 also shows over all similar order of magnitude and axial trends for TKE and k_{sgs} .

In summary, this section dealt with statistically stationary cases of single and two phase gas jets. LES was shown to provide good agreement with experimental results in predicting mean and rms quantities. The sub-grid spray source was then analyzed. Finally, a comparison between the sub-grid and turbulence kinetic energies was discussed.

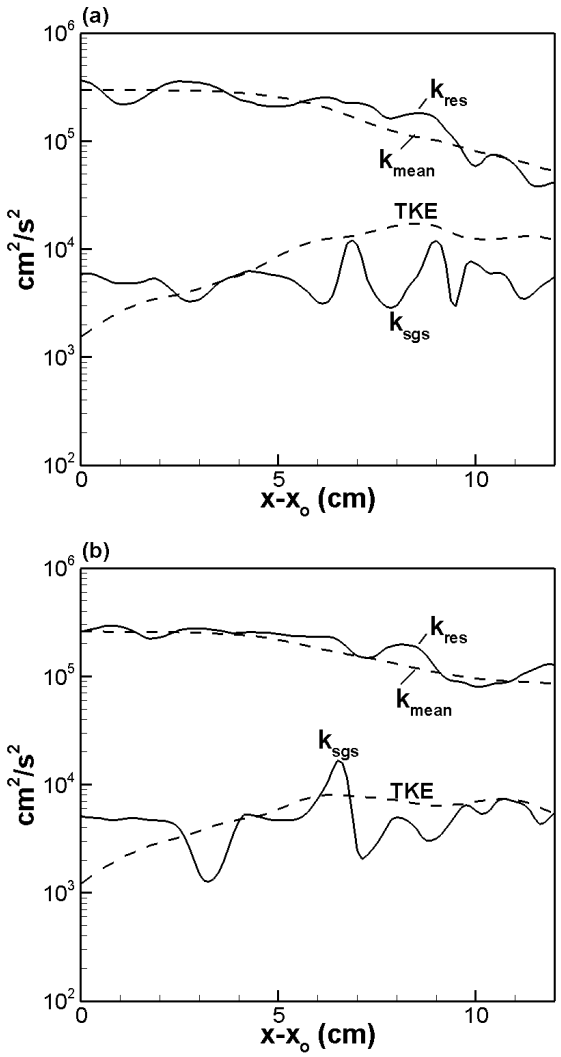

Figure 5 Centerline axial profiles of resolved, sub-grid, mean and turbulent (rms) kinetic energies: (a) single phase jet and (b) two phase jet. The profiles are shown at a specific time arbitrarily selected during the stationary stage of the jet.

Non-evaporative Diesel Sprays

This section now extends the ongoing discussion of sub-grid scale two-phase turbulence interaction to non-evaporative high speed diesel spray simulations. The LES results are compared with the near nozzle X-ray radiography line-of-sight measurements (Kastengren et al, 2007a and 2007b) for non-evaporative diesel sprays. The resolution of the X-ray experiments depends upon the beam size which was 470 μm in the spray injection

direction and 80 μm in the transverse direction.

Figure 6 shows a schematic of the experimental set-up. The beam is collected on a photodiode after passing through the diesel spray. The photodiode measures the incident intensity of the X-ray beam. This intensity (I) and the intensity at the photodiode with the spray shut-off (I_o) are used in an absorption based formula to obtain the spray mass in the beam's line of sight. As shown in this figure the measurements are performed at several axial and radial locations in the spray. Each measurement provides the integrated spray mass along the X-ray beam path. The projected mass density is then obtained by normalizing the spray mass with the beam cross-sectional area. A collection of these measurements results in a two-dimensional distribution of spray mass in a plane perpendicular to the beam. The measurements were conducted for a hydroground and a non-hydroground nozzle. However no such distinction was possible in the present simulation, since the injector nozzle flow was not simulated.

The simulations were performed in a cylinder with a diameter of 2 cm and length of 10 cm. With the nozzle located at $z = 0$, the comparisons with the experiments are made at axial distances of $z = 0.2$ mm, 10 mm, and 20 mm. The computational grids used for these simulations are shown in Table 2. The ambient is filled with N_2 at atmospheric pressure, and the spray is injected at 250 bar with an injection duration of 1.0 ms. The experimental time varying spray velocity at $z = 0.2$ mm was prescribed as the injection velocity for the simulations (see Figure 7). This method provided an accurate representation of the experiments, and was possible since the location of the nozzle exit plane coincided with the $z = 0.2$ mm location for the computational cell sizes considered here. The experiments used diesel calibration fuel which was simulated using Tetradecane ($C_{14}H_{30}$) in the calculations.

A recently developed gas-jet model by Abani *et al.* [22] is also explored in the results. The gas-jet model serves to reduce the grid dependencies associated with the spray-ambient coupling. The simulation on the intermediate Grid-B is the basis of all the comparisons in this section. Unless otherwise mentioned, all LES runs include the LES spray source model discussed earlier in this paper. A primary objective of this section is to compare and validate the LES spray results against the near nozzle experimental spray data.

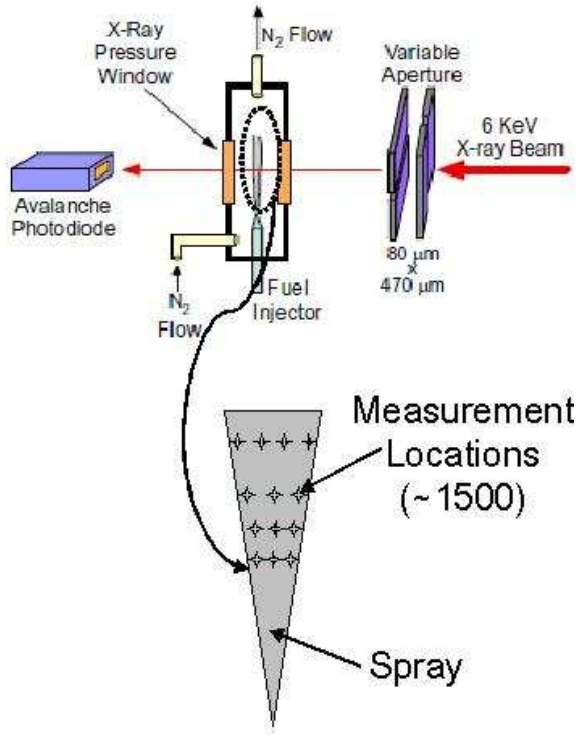

Figure 6. Schematic of experimental line of sight measurements which results in a two-dimensional spray structure (schematic taken from Powell *et al* [23])

Table 2. Computational grids for non-evaporative spray study

Grid	N_xxN_yxN_z	$\Delta x(=\Delta y)$ (mm)	Δz (mm)
A	30x30x150	0.67	0.67
B	30x30x300	0.67	0.33
C	60x60x300	0.33	0.33

Figure 8 compares contour plots of projected mass density between experiments and the LES run with Grid-B. Even though the radial grid resolution in simulation (0.66 mm) is much coarser than the optical resolution of experiments (0.08 mm) and the nozzle diameter (0.183 mm), this computational grid is reasonably fine in the context of practical diesel engine simulations. Considering such a thin spray zone is being resolved with a relatively coarse grid, it is encouraging to observe that the simulation is able to provide a reasonable estimate of the spray length and the spray head structure in comparison with the experiment.

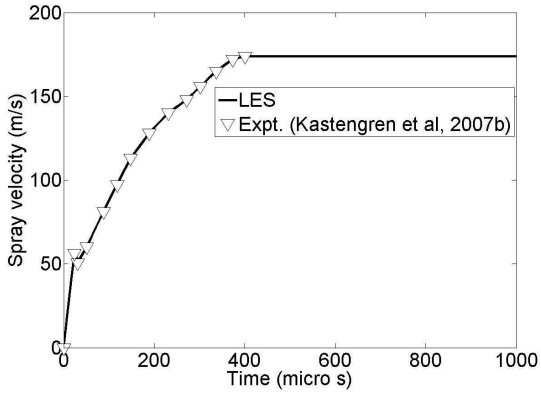

Figure 7. Spray velocity boundary condition at injector: Experimental velocity profile at z=0.2 mm was assigned at injector exit plane for simulation

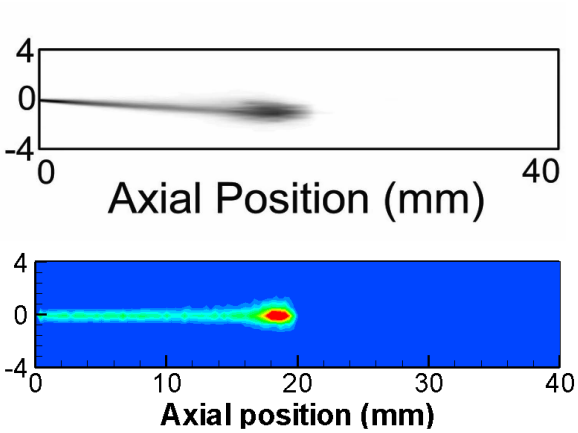

Figure 8. Projected mass density contours from experiment (top) and simulation (bottom) at $t = 331\ \mu s$. Contour values are between 0 and 100 $\mu g/mm^2$.

Figure 9 shows experimental and predicted projected density profiles at $z = 10$ mm and $t = 376\ \mu s$. The LES results shown in this figure include: (a) Grid-B run with the spray source model, (b) Grid-B run without the spray source model and (c) Grid-C run with the spray source model. In these results each symbol represents a grid cell. This figure shows that the additional cells in Grid-C simulation provide a good comparison of the projected density values with the experimental profile. The Grid-B LES simulation with the spray source model gives a good prediction of the centerline peak projected density value and the spray width. For Grid-B, the first grid cell next to the centerline is beyond a significant portion of the spray half-width, and therefore a good estimate of the centerline peak projected density value is considered a significant achievement of the present LES. Note that the LES results on either side of the spray axis are asymmetric due to the unsteady nature of the flow. To assess the importance of the spray source model, the projected mass density profile from Grid-B without the spray source model is also shown in Figure 9. It can be seen that without the spray source model the peak projected density is under-predicted. The inclusion of the spray source model increases turbulence dispersion of the droplets in the surrounding ambient. Therefore, in comparison with the simulation without the spray source model, the simulation with the spray source model results in a higher momentum loss leading to an increased projected density at any given axial location.

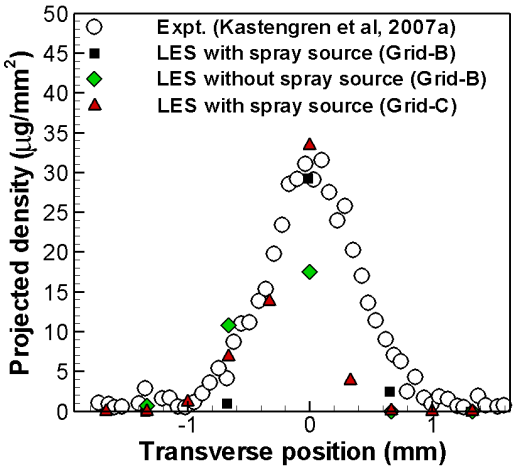

Figure 9. Projected density profiles at an axial distance $z = 10$ mm and time $t = 376\ \mu s$

The projected density [$\mu g/mm^2$] is integrated in the transverse direction to obtain the transverse integrated mass (TIM) [$\mu g/mm$] as a function of the axial distance. Figure 10 shows experimental comparisons of the LES TIM evolutions at three different axial locations for (a) Grids A and (b) Grid B. This figure also shows results from an additional simulation that uses the gas-jet model [22].

Figure 10 shows that the simulation results can accurately predict the important spray characteristics such as the times when the spray reaches a particular axial location and the time rates of increase and decrease of TIM. The peaks of TIM are somewhat over predicted by the simulation which is acceptable since the experimental results are ensembled whereas the LES results are unsteady and contain higher fluctuations. The simulation result from the coarser grid, Grid-A, reduce fluctuation effect in the TIM profile and provide a better comparison for the peak value (see Figure 10(b)). However, the evolution profile of TIM is not significantly different between the two grids. An inclusion of the gas-jet model reduces the grid dependencies and provides similar TIM evolution

between Grids A and B. The TIM evolution profile with the gas-jet model is very similar to that without the gas jet model, except a reduction in the peak TIM value with the gas jet model.

(a)

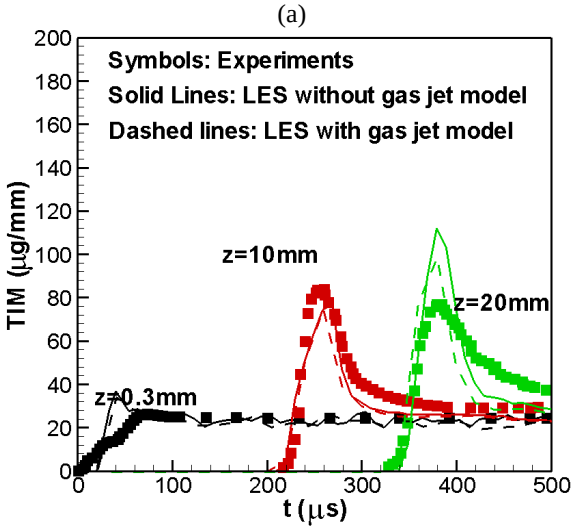

(b)

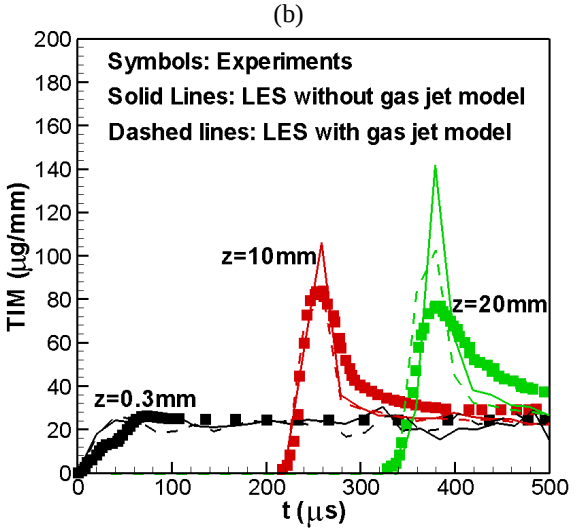

Figure 10. Transverse integrated mass (TIM) comparison between experiments and simulation for (a) Grid A and (b) Grid B

Figure 11 shows the LES predicted time evolution (or, trajectory) profiles of the peak TIM location from simulations with and without the gas-jet model. The slope of this trajectory can be interpreted as the inverse spray penetration speed. These figures show that the results with and without the gas-jet model are very similar, with a higher spray penetration speed when the gas jet model is used.

Figure 12 shows evolution of the global spray axial momentum. The LES results with and without the gas jet model are shown. There is a very good comparison between LES and experiments for global spray momentum evolution. The use of the gas-jet model results in a slightly higher momentum. Also, as mentioned previously, simulation results make no distinction between the hydroground and non-hydroground nozzles results.

(a)

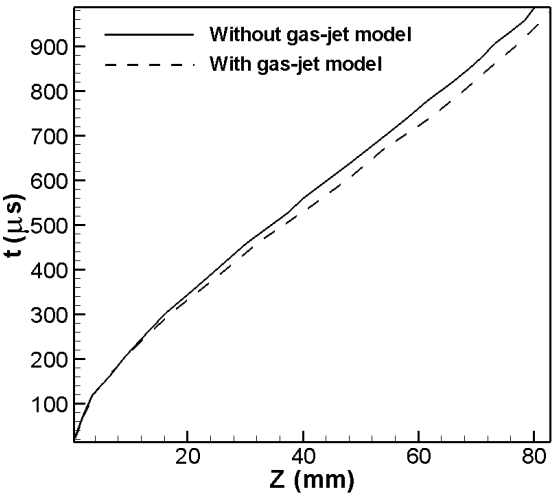

Figure 11. Trajectory of peak TIM location from the LES run on Grid-B

(b)

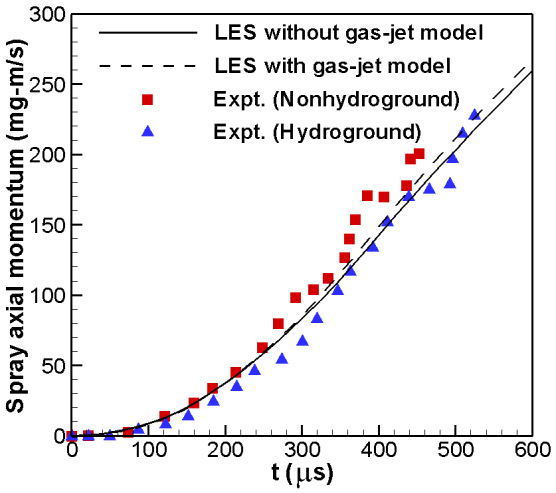

Figure 12. Evolution of global axial momentum.

Figure 13 compares axial profiles of mass averaged axial velocity between LES and experiment. LES results without the gas-jet model are shown in Figure 13(a), and with the gas-jet model are shown in Figure 13(b). The experimental results are shown for $t = 438\ \mu s$. In order to make a reasonable comparison between the instantaneous LES results and the ensemble experimental results, a time evolution of this

profile is shown for simulations between $380\ \mu s < t < 480\ \mu s$ an intervals of $20\ \mu s$.

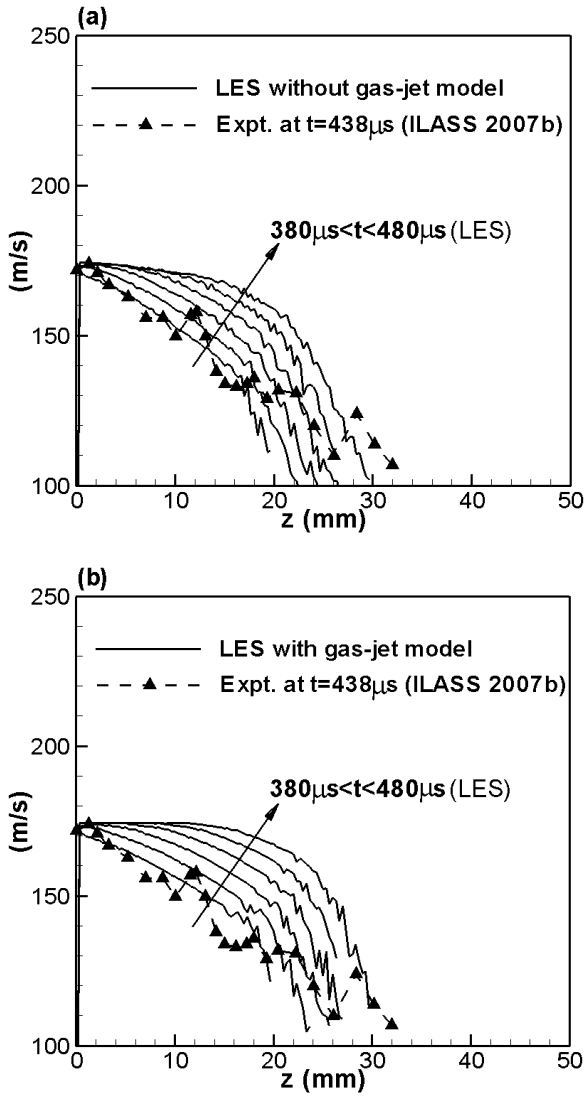

Figure 13. Mass averaged axial velocity profile from experiments (symbols) and LES (lines). LES results are shown between $380\ \mu s < t < 480\ \mu s$ at an interval of $20\ \mu s$.

Figure 13 shows that at $438\ \mu s$ the simulation predictions show the spray is still evolving. At later times, at its quasi steady state, the spray velocities from the simulations are higher than those from experiments. The LES results with the gas jet model are flatter in the near nozzle region and deviate more from the experimental profile. Fro these results the LES results without the gas-jet model provid a better prediction. It is important to mention that the experimental axial spray velocity is obtained after applying further calculations on the measured data. These calculations involved application of a control volume approach on flow continuity and numerical integration over curve fits. Hence the comparison of spray velocity between LES and experiments is reasonably good considering experimental uncertainties and a relatively coarse nature of the computational grid (see Figure 9). It is expected that improvements in the primary break-up would be a key factor in obtaining more accurate near nozzle results on the similar type of grids.

From Figures 10 to 13, it is concluded that the results obtained with the gas-jet model are not significantly different from the results without the gas-jet model. The gas-jet model has been found to be useful in spray prediction on very coarse grids, e.g., grid sizes greater than 1-2 mm [22] in the context of RANS diesel spray simulations. A future study is suggested to further explore the effect of the gas-jet model on coarse grid LES of diesel engines.

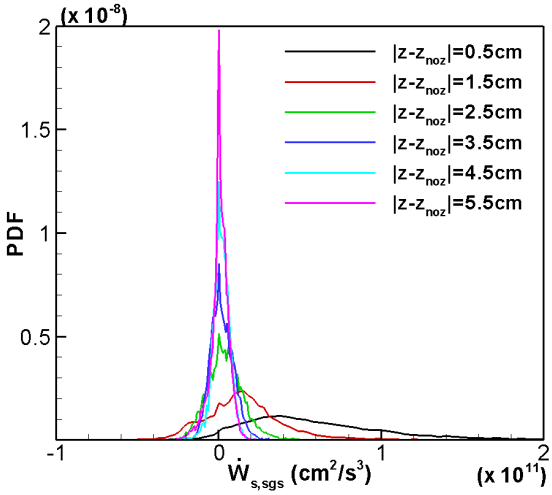

Figure 14. PDF of spray source term at several axial locations. Each PDF profile is based on the droplets within an axial width of 1cm centered at the indicated location

Figure 14 shows PDF plots of the spray source term at various axial locations downstream of the spray nozzle. This figure shows that the shapes of these PDFs are similar to those observed in the particle laden jet configuration but the magnitudes change significantly downstream. The droplet size distribution does not change much axially in the particle laden jet, whereas it changes significantly in sprays due to primary and secondary break-up processes. The PDF plots show that in the near nozzle region the spray is a significant source of sub-grid kinetic energy, whereas at the downstream locations the distribution of $\dot{W}_{s,sgs}$ is

symmetric on positive and negative sides with much smaller magnitudes. This indicates the isotropic nature of the sub-grid scale droplet ambient interaction at downstream locations.

Conclusions

This paper presented LES results for a particle laden gas jet and non-evaporative diesel sprays. The simulations results were compared with experiments. The primary focus of the study was to explore the capability of LES in predicting two-phase interaction with a focus on the modeling of the sub-grid scale droplet effects on turbulent kinetic energy.

For stationary jet cases, the LES results were found to provide very good predictions of the mean and rms quantities in comparison with previous experiments. The shifting distribution the LES spray source term from negative to positive direction was discussed.

Non-evaporative diesel spray results from LES were found to compare with experiments reasonably well at near injector locations. At such locations, the spray is too thin (< 1-2 mm) to be adequately resolved with computational cells, and a very important role is played by the spray models. A good experimental comparison for peak projected density and transverse spray width (~1.5mm) was obtained from LES on relatively coarse mesh ($\Delta x = 0.67\text{mm}$). Without the LES spray source model, the comparison was shown to become poorer. The LES comparisons with experiments were also made for spatial time evolution profiles of transverse integrated mass, mass averaged axial velocity and global axial momentum. All results show a good agreement. It was shown that a high speed diesel spray can create significant energy at the sub-grid scale in the near nozzle region. This sub-grid kinetic energy is important in the models of sub-grid shear stress and droplet turbulent dispersion.

Acknowledgements

The authors would like to thank General Motors Research and Development for their support through the GM-UW Co-operative research Lab. The insightful comments from Dr. Shengming Chang (currently at CD-adapco) are appreciated. The authors would also like to acknowledge Dr. Christopher F. Powell and Dr. Alan L. Kastengren (both at Argonne National Laboratory, Chicago) for providing their X-ray radiography data and invaluable feedback.

References

1. Armenio, V., U. Piomelli. and V. Fiorotto, “Effect of subgrid scales in particle motion”, *Physics of Fluids*, 11(10), pp 3030-3042, 1999
2. Okong’o. N., and J. Bellan, “Consistent large-eddy simulation of a temporal mixing layer laden with evaporating drops. Part 1. Direct numerical simulation, formulation and a priori analysis”, *Journal of Fluid Mechanics*, 499, pp 1-47, 2004.
3. Leboissetier, A., Okong'o, N. and Bellan, J., “Large Eddy Simulation of jets laden with evaporating drops”, 42nd AIAA Aerospace Sciences Meeting and Exhibit, January 5, 2004 - January 8.
4. Leboissetier, A., N. Okong’o., and J. Bellan, “Consistent large-eddy simulation of a temporal mixing layer laden with evaporating drops. Part 2. A posteriori modelling”, *Journal of Fluid Mechanics*, 523, pp 37-78, 2005.
5. Stolz, S. and Adams, N. A., “An approximate deconvolution procedure for large-eddy simulation”, *Phys. Fluids* 11, 1699-701, 1999.
6. Stolz, S., N. A. Adams, and L. Kleiser, “An approximate deconvolution model for large-eddy simulation with application to incompressible wall-bounded flows”, *Physics of Fluids*, 3, pp 997-1015, 2001.
7. Shotorban, B., and Mashayek F., “Modeling subgrid-scale effects on particles by approximate deconvolution”, *Physics of Fluids*, 17, 2005.
8. Shotorban, B., K. K. Q. Zhang, and F. Mashayek, “Improvement of particle concentration prediction in large-eddy simulation by defiltering”, *International Journal of Heat and Mass Transfer*, 50, pp 3728-3739, 2007.
9. Bharadwaj, N., Chang, S., and Rutland, C. J., “Large eddy simulation modelling of spray-induced turbulence effects”, *Int. J. Engine Res.*, 10(2), 2009.
10. Sirignano, W. S., “Volume averaging for the analysis of turbulent spray flows”, *International Journal of Multiphase Flows*, 31, pp 675-705, 2005.
11. Pomraning, E., and C. J. Rutland, “Dynamic one-equation nonviscosity large-eddy simulation model”, *AIAA Journal*, 40(4), 689-701, 2002.
12. Gillandt, I., Fritsching, U. and Bauckhage, K., “Measurement of phase interaction in dispersed gas/particle two-phase flow”, *Int. J. Multiphase Flow*, 27, 1313-1332, 2001.
13. Kastengren, A. L, Powell C. F, Cheong S. K., Wang, Y, Im KS, Liu, Xin, Wang, J., “Determination of diesel spray axial velocity using

X-ray radiography", *SAE Paper 2007-01-0666*, (2007a).

14. Kastengren, A. L., Powell, C. F., Wang, Y., Im, K., Liu X., Cheong, S. K., and Wang, J., "Improved method to determine spray axial velocity using X-ray radiography", *20th annual conference on liquid atomization and spray systems, Chicago, IL, May 2007* (2007b).
15. Amsden, A. A., "KIVA-III: A KIVA program with blocked structure mesh for complex geometries", Los Alamos National Laboratory, LA-12503-MS, 1993.
16. Amsden, A. A., "KIVA-II: A computer program for chemically reactive flows with sprays", Los Alamos National Laboratory, LA-11560-MS, 1989
17. Germano, M., U. Piomelli, P. Moin, and W. H. Cabot, "A dynamic sub-grid scale eddy viscosity model", *Physics of Fluids*, pp 1760-1765, 1991
18. Menon, S., "Subgrid combustion modelling for large-eddy simulations", *Int. J. of Engine Research* 1, 2000.
19. Beale, J. C., and Reitz, R. D., "Modeling spray atomization with Kelvin-Helmoltz/Rayleigh-Taylor hybrid model", *Atomization and Sprays*, pp 632-650, 1999.
20. O' Rourke, P. J., "Collective drop effects on vaporizing liquid sprays", PhD Thesis, Princeton University, 1981.
21. Reitz, R., "Modeling atomization process in high-pressure vaporizing sprays", *Atomization and Sprays*, 3(4), pp 309-337, 1987.
22. Abani, N., Munnannur, A., & Reitz, R. D., "Reduction of numerical parameter dependencies in diesel spray models". *Journal of Engineering for Gas Turbines and Power, 130*, 032809, 2008.
23. Powell, C. F., Ciatti S. A., Cheong, S. K., Liu, J., and Wang, J., "X-ray absorption measurements of diesel sprays and the effects of nozzle geometry", SAE paper 2004-01-2011.